2016

Compact Refrigeration System For Electronics Cooling Based on a Novel Two-Phase Jet Impingement Heat Sink

Pablo de Oliveira
Federal University of Santa Catarina, Brazil, pablo_oliveira@polo.ufsc.br

Jader Barbosa
Federal University of Santa Catarina, Brazil, jrb@polo.ufsc.br

Compact Refrigeration System For Electronics Cooling Based on a Novel Two-Phase Jet Impingement Heat Sink

Pablo A. de OLIVEIRA, Jader R. BARBOSA Jr. *

Polo -- Research Laboratories for Emerging Technologies in Cooling and Thermophysics
Department of Mechanical Engineering, Federal University of Santa Catarina
Florianópolis, Santa Catarina, Brazil
E-mail: jrb@polo.ufsc.br

* Corresponding Author

ABSTRACT

The performance of a compact vapor compression cooling system equipped with a R-134a small-scale oil-free compressor and a novel heat sink that integrates, into a single unit, the evaporator and the expansion device was experimentally evaluated. The expansion device can be a single orifice or an array of orifices responsible for the generation of a high-speed two-phase jet impinging on a heated surface. A comparison between the performance of the proposed refrigeration system operating with single and multiple jets is presented and the influence of the following parameters is quantified: (i) thermal load applied on the heat sink, (ii) number of orifices and (iii) geometrical arrangement of the orifices (jets). The analysis is based on thermodynamic performance metrics (coefficient of performance, second-law efficiency and second-law ratio) and steady-state heat transfer parameters (surface temperature and average heat transfer coefficient) associated with the impinging jet(s) for single and multiple orifice tests. The two-phase jet heat sink was capable of dissipating cooling loads of up to 160 W and 200 W from a 6.36-cm^2 surface for single and multiple orifice configurations, respectively. For these cases, the temperature of the impingement surface was kept below 40ºC and the average heat transfer coefficient reached values between 14,000 and 16,000 W/(m^2K). The proposed compact vapor compression cooling solution can be further developed for specific applications in thermal management of power electronics for a variety of stationary and mobile systems.

1. INTRODUCTION

Thermal management devices for high heat flux applications such as high-performance computers, high-power electronic modules and hybrid/electric vehicles power equipment have been under intense research over the past three decades (Mudawar *et al.*, 2001; Chu *et al.*, 2004; Nakayama *et al.*, 2009). The proper functioning and reliability of electronic components depends heavily on adequate thermal management. The principal vector of failure in electronic components during operation is temperature (55%), followed by vibration (20%), humidity (19%) and dust (6%) (Anandan & Ramalingam, 2008). Advances in micro-fabrication of electronic circuitry have led to a continual decrease in size allowing more circuit components per unit surface area, which severely increases the heating power density. The growing complexity that characterizes the current design of electronic components associated with the ever-increasing power consumption and the continuous scale reduction of these devices place thermal management of electronics as one of the most strategic challenges for technological innovation in heat transfer (Bar-Cohen, 2013).

Conventional techniques for electronics cooling encompass finned heat sinks and cold plates for which single-phase heat transfer with air or liquid flow is the main cooling mechanism. Several researchers agree that those schemes will no longer be capable of maintaining the operating temperatures of processors and other high-power components below tolerable levels (Ortega & Birle, 2006; Whelan *et al.*, 2012; Mancin *et al.*, 2013). Therefore, new concepts for the removal of high heat fluxes are required so as to meet the increasing demands with greater efficiencies.

According to Barbosa *et al.* (2012), there is a clear understanding that mechanical vapor compression refrigeration is among the most promising *active* cooling technologies (i.e., those capable of lowering the chip temperature below that of the ambient) for the next generation of electronic systems. In contrast with the currently available passive cooling techniques (heat pipes and single-phase liquid loops), sprays, two-phase impinging jets and boiling in microchannels can be easily integrated with vapor compression cooling to achieve below-ambient junction temperatures.

Amongst the direct liquid cooling techniques that use enhanced heat transfer (sprays and two-phase jets), spray cooling devices have been successfully integrated with mechanical vapor compression systems (Yan *et al.*, 2010; Chunqiang *et al.*, 2012; Xie *et al.*, 2014; Hou *et al.*, 2015). However, as far as the present authors are aware, an active cooling system that integrates two-phase impinging jets and mechanical vapor compression refrigeration has not yet been reported in the literature. Besides, none of these works devoted specific attention to the full potential size reduction (miniaturization) of the cooling system, either by using a small-scale compressor or by designing a truly compact cooler unit.

This paper proposes a new compact cooling system with potential applications in thermal management of electronic devices. The main components of the system are a linear oil-free small-scale compressor and a compact cooling module that combines an array of micro-orifices (the expansion device) and a jet-impingement-based heat sink (evaporator) into a single unit. The system operates with R-134a, as this was the refrigerant for which the compressor has been designed. The experimental evaluation of the proposed system quantifies the influence of the thermal load, number and array (geometrical configuration) of orifices on the system performance. The analysis is based on thermodynamic performance metrics and steady-state heat transfer parameters associated with the impinging jet(s) for single and multiple jet cooling tests.

2. EXPERIMENTAL WORK

2.1 Experimental Facility

A schematic diagram of the experimental apparatus is shown in Fig. 1. A small-scale (0.27 cm^3 maximum volumetric displacement, 340 Hz operating frequency, 1.3 kg total weight) linear-motor compressor was used. The compressor was manufactured by Embraco and designed to operate with R-134a. It was equipped with a frequency inverter to control the volumetric displacement (piston stroke). A digital power meter was employed to measure the electrical power consumption of the compressor. The compressor was positioned inside a purpose-built calorimeter which was developed to indirectly measure the heat dissipation rate through the compressor shell, thus providing closure for the overall system energy balance. The calorimeter design and modeling are presented in detail in Oliveira (2016).

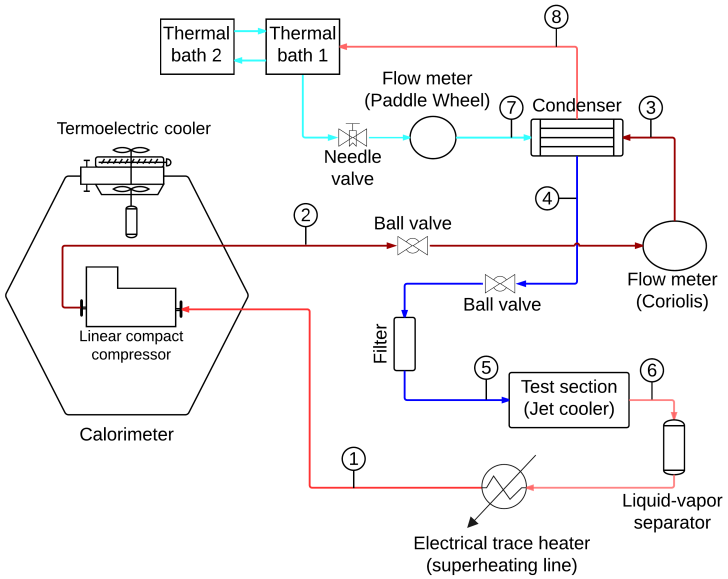

Figure 1: Schematic representation of the experimental apparatus. (1) Compressor inlet (suction); (2) Compressor outlet (discharge); (3) Condenser inlet (refrigerant side); (4) Condenser outlet (refrigerant side); (5) Jet cooler inlet; (6) Jet cooler outlet; (7) Condenser inlet (WEG side), and (8) Condenser outlet (WEG side).

A Coriolis mass flow meter was placed downstream of the compressor to measure the R-134a mass flow rate. A compact brazed plate counter-flow heat exchanger was used as a condenser. The volumetric flow rate of the secondary fluid (water-ethylene glycol - WEG - mixture) was measured with a paddle wheel flow meter. The temperature of the

WEG mixture at the condenser inlet was maintained a fixed by two cascade thermal baths. Absolute pressure transducers and resistance temperature detectors (RTDs) were used to measure the local values of pressure and temperature in the apparatus. Although an air-cooled condenser might have been a more suitable choice in a real application, a liquid-cooled condenser was used in the present test apparatus to facilitate the evaluation of the system performance under different operating conditions, particularly the hot reservoir (ambient) temperature.

The two-phase jet cooler (test section) is presented in Fig. 2. Figure 2 (a) shows a photograph of the assembly and Figs. 2 (b), (c) and (d) show some individual components of the jet cooler. The high-pressure sub-cooled liquid from the condenser flows through the top of the test section (metallic cap) into the internal orifice plenum – see Fig. 2 (c). The expansion device is an array of 10-mm long polyacetal resin (POM) threaded screws with the actual orifices drilled along their center lines. The screws are fastened into a POM orifice plate so that several combinations of orifices (jet array configurations) can be tested. Dummy screws occupy the remaining positions.

As the jets expand in the jet chamber, Fig. 2 (b), they impinge vertically on the top surface of a heated cylindrical copper block. The area of the circular target surface is 6.36 cm^2. The copper block is mounted vertically in a polycarbonate bottom piece, Fig. 2 (d), designed to thermally insulate the sides and bottom of the block and facilitate liquid drainage from the jet chamber into a liquid-vapor separator (suction-line accumulator) positioned below the jet cooler. The heat source is a 200-W skin (film) heater placed below the copper block. Five RTDs are introduced in the copper block to measure the temperature and allow for an estimate of the surface temperature to be made using Fourier's law. The external dimensions of the two-phase jet cooler in Fig. 2 (a) are 80 mm in width and depth × 112.5 mm in height.

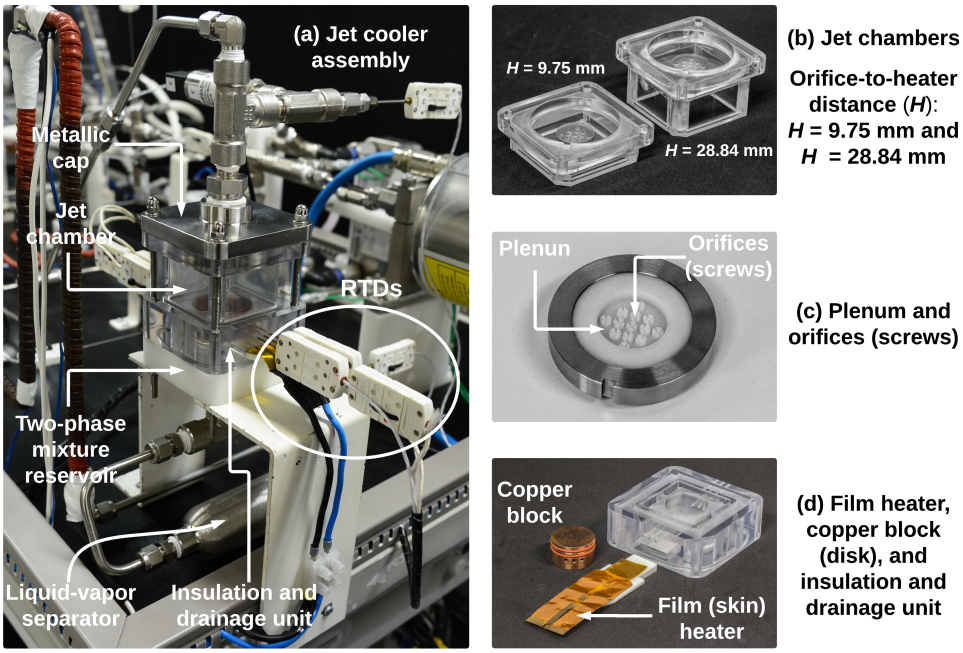

Figure 2: Photograph of the two-phase jet cooler, i.e., assembly and some individual components.

The superheating line downstream of the jet cooler is composed of an electrical trace heater wrapped around the compressor suction line. This guarantees the refrigerant superheating degree at the compressor inlet required for a safe operation of the compressor. As in other high-thermal performance heat sinks, such as microchannel heat exchangers (Marcinichen *et al.*, 2013), the heat sink overall thermal conductance decreases significantly as the outlet vapor quality increases. Thus, to generate the high heat transfer coefficients required to remove the high heat fluxes and maintain a low surface temperature, there must be a significant liquid fraction at the outlet of the heat sink. In a laboratory test device such as the present facility, Joule heating is the preferred mode of supply of the superheating input thermal power due to its low cost and simple control. However, in a real application, the superheating thermal energy may come from another heat transfer process (Hou *et al.*, 2015) or from an internal heat exchanger (Barbosa & Hermes, 2006), not necessarily adding to the electrical supply to the system.

Regarding the variable control strategies, the thermal load imposed on the refrigeration system was provided and finely

controlled by a DC digital power supply. During the experimental runs, the thermal load was increased by increasing the voltage or the current provided by the power supply. A split-type air conditioner controlled the room temperature and the internal temperature of the calorimeter was finely controlled by the combined action of a thermoelectric cooler, an air heater, centrifugal fans and dedicated hardware and software, i.e., a built-in LabVIEW PID controller code which operates coupled with a specially designed voltage-to-current converter electronic board. Besides, the temperature of point 1 (compressor inlet in Fig. 1) was accurately controlled using the same dedicated hardware and software. Therefore, at steady state, it was possible to maintain a fixed refrigerant superheating degree at the compressor inlet.

2.2 Experimental Conditions

The experimental tests were run at the maximum compressor displacement. The diameter of the orifices was 300 μm and the orifice-to-heater distance (jet length) was 28.84 mm – see Fig. 2 (b). The secondary fluid temperature was set at 25ºC in all tests. The refrigerant charge in the system was adjusted so that the tests for each multiple jet array had the same refrigerant mass flow rate at the lowest thermal load (75 W). All experimental runs were carried out in the heating-up mode, i.e., increasing the heat load until the critical heat flux was reached. The influence of the following variables was investigated: (i) applied thermal load, (ii) number of orifices and (iii) orifice array configuration (for the tests with multiple jets). Figure 3 presents the single and the multiple jet arrays explored, which are different combinations of a five-orifice configuration.

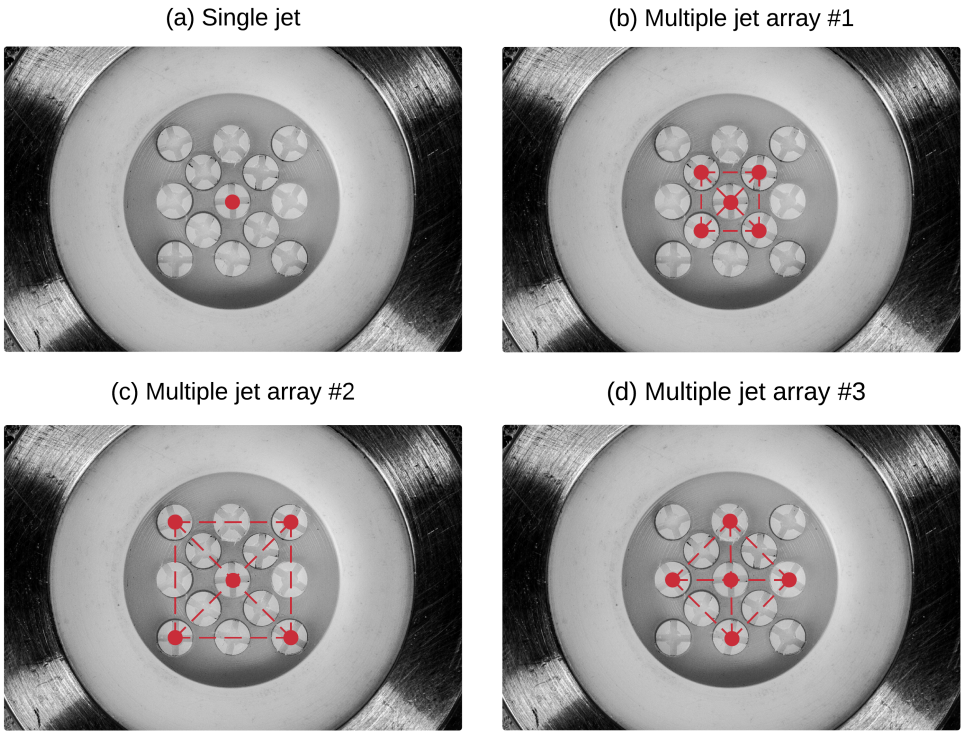

Figure 3: Internal orifice plenum showing the (a) single and (b)-(d) multiple orifice configurations.

In all experimental tests, the mass flow rate of the WEG mixture was kept fixed at 180 kg/h, the room temperature and the calorimeter internal temperature were set at 25ºC and the compressor inlet superheat, defined as $\Delta T_{sup} = T_{comp,i} - T_{evap}$, was kept fixed at 10ºC.

The output (dependent) variables of the experimental apparatus are the refrigerant mass flow rate, pressures, temperatures, refrigerant sub-cooling degree at the outlet of the condenser, vapor mass quality at the outlet of the two-phase jet cooler, heat transfer rates and compressor power. Based on the output variables, the jet impingement heat transfer coefficient and the system performance metrics (to be defined) can be calculated. The criteria to determine the steady-state operation of the experimental apparatus and the experimental uncertainties of the independent and dependent parameters (with their calculation procedure) are presented and discussed in detail in Oliveira (2016).

3. DEPENDENT VARIABLES AND PERFORMANCE METRICS

The refrigerant enthalpy at the outlet of the two-phase jet cooler, h_6, can be calculated from the energy balance on the cooler neglecting the kinetic and potential energy contributions as follows:

$$h_6 = h_5 + \frac{\dot{Q}_c}{\dot{m}_r} \tag{1}$$

where $\dot{m}_r$ is the refrigerant mass flow rate, $\dot{Q}_c$ is the cooling capacity and h_5 is the refrigerant specific enthalpy at the inlet of the two-phase jet cooler, respectively. The enthalpies were computed via REFPROP 8.0 (Lemmon *et al.*, 2007) using the local experimental values of pressure and temperature.

The vapor mass quality at the exit of the two-phase jet cooler, x_6, was determined using h_6 and the measured outlet pressure, P_6. The saturation pressures were calculated directly from the experimental data, i.e., $P_{evap} = P_6$ and $P_{cond} = P_4$, both taken at the outlets of the jet heat sink and condenser, respectively. The average jet impingement (surface) heat transfer coefficient, φ, is a key parameter in the design of the two-phase jet cooler. It is defined by:

$$\varphi = \frac{\dot{Q}_c^*}{A_s(T_s - T_{evap})} \tag{2}$$

where $\dot{Q}_c^*$ is the corrected cooling capacity, i.e., the useful fraction of the input power to the skin heater, $\dot{W}_{hl}$, that actually reaches the impingement surface. A numerical simulation of the heat transfer in the jet cooler using a commercial software package revealed that approximately 95% of $\dot{W}_{hl}$ reaches the impinging surface (Oliveira, 2016).

The temperature of the top (impingement) surface of the copper block, T_s, was determined through a linear extrapolation of Fourier's Law considering an one-dimensional heat conduction in the axial direction,

$$T_s = \overline{T}_{RTD} - \frac{L_s \dot{Q}_c^*}{A_s k_s} \tag{3}$$

where L_s is the distance between the top surface of the copper block and the plane of the RTDs inside the copper block, $A_s = (\pi D^2)/4$ is the surface impingement area, D is the diameter of the impinging surface and k_s is the copper thermal conductivity evaluated at $\overline{T}_{RTD}$, which is the arithmetic mean of the five RTDs used to measure the copper block temperature.

The performance metrics of the present refrigeration system are defined based on the cooling capacity, energy transfer rates imposed on the system and the associated thermal resistances. Three performance metrics are introduced to support the present analysis. The first one is the coefficient of performance considering the energy consumption strictly necessary to remove the imposed heat load upon the jet cooler, COP_{jc}:

$$COP_{jc} = \frac{\dot{Q}_c}{\dot{W}_{comp} + \dot{W}_{fan}} \tag{4}$$

where $\dot{W}_{comp}$ and $\dot{W}_{fan}$ are the electrical power consumptions of the compressor and DC centrifugal fan used to cool the compressor shell, respectively. $\dot{W}_{fan}$ is an averaged value obtained from repeated power (voltage and current) measurements using two digital multimeters.

The second performance metric is the second-law efficiency, η. This parameter can help to quantify the external irreversibilities in the system, i.e., those linked to the heat transfer with finite temperature differences in the heat exchangers. It is defined as the ratio of the coefficient of performance of the actual refrigeration system to that obtained assuming an ideal cooling device operating with real heat exchangers,

$$\eta_{jc} = \frac{COP_{jc}}{COP_{id}} \tag{5}$$

where COP_{id} is the ideal (Carnot) coefficient of performance based on saturation temperatures of the refrigerant in the condenser and evaporator (two-phase jet heat sink).

The third performance metric accounts for the internal and external irreversibilities in the refrigeration system. Miner and Ghoshal (2006) pointed out the inability of the second-law efficiency alone to capture the effects of performance degradation that arise from the resistances to heat flow into the active cooler near the heat sink, R_{hs}, and out of it near the hot-side reservoir (ambient), R_{amb}. Based on the thermal analysis of a passive cooling system and using the concept of thermal resistance, they derived a relationship for the minimum second-law efficiency, η_{min}, that an active cooling system must exhibit to perform equally as well as an *identical system without active cooling*. This is given by,

$$\eta_{min} = \frac{T_s - T_{w,i}}{\left(\frac{R_{hs}}{R_{amb}}\right) T_{w,i} + T_s} \tag{6}$$

where $T_{w,i}$ is the hot reservoir temperature and the thermal resistances R_{hs} and R_{amb} are, respectively, given by,

$$R_{hs} = \frac{T_s - T_{evap}}{\dot{Q}_c} \tag{7}$$

$$R_{amb} = \frac{T_{cond} - T_{w,i}}{\dot{Q}_c + \dot{W}_{comp} + \dot{W}_{fan}} \tag{8}$$

A second-law ratio, η^*, can be introduced to evaluate how efficient the active cooling system is in comparison with its passive counterpart. This third metric allows one to to better evaluate the merits of moving from *simple passive cooling* to an *active cooling solution*, which is defined as,

$$\eta^*_{jc} = \frac{\eta_{jc}}{\eta_{min}} \tag{9}$$

4. RESULTS

The coefficient of performance is shown in Fig. 4 (a). A quasi-linear increase of COP_{jc} with $\dot{Q}_c$ is observed, which results mainly from the increase of $\dot{Q}_c$ since $\dot{W}_{comp}$ increases slightly as depicted in Fig. 4 (b). The refrigeration system performs better with the multiple jet cooling strategy, particularly for arrays #2 and #3, since $\dot{W}_{comp}$ is smaller for these cases. Figure 4 (a) also shows that for higher cooling capacities, the multiple jet strategy decisively contributed for the cooling system to perform better. Besides being capable of removing higher heat loads from the impingement surface (up to 200 W), COP_{jc} was higher compared to the single jet case. No noticeable differences are perceived for COP_{jc} regarding the multiple jet arrays #2 and #3. On the other hand, the multiple jet array #1 shows lower COP_{jc} values because of the higher compressor power consumption, as depicted in Fig. 4 (b). Considering the trends of the curves in Fig. 4 (a), the performance of the system is expected to increase significantly at higher cooling capacities, indicating that the proposed active cooling system can be a suitable alternative for high heat flux removal. The heat dissipation rate through the compressor shell was quantified via both calorimeter measurements and compressor energy balance (Oliveira, 2016). For the tests reported here, the average and maximum values of the relative difference between the two methods are 6.4% and 13%, respectively. Hence, heat leaks in the experimental facility can be considered negligible.

Figure 5 (a) presents the behavior of the evaporating and condensing temperatures as a function of the cooling capacity. The geometry of the multiple jet arrays seems to affect very weakly the saturation temperatures, since no significant differences were observed between the three configurations. The considerably lower temperature values compared with those observed in the single jet cooling case can be explained by the decrease of the saturation pressures, which is a result of the lower restriction imposed by the multiple orifices with a flow area five times larger than that of the single orifice.

The second-law ratio confirms the superior performance of the multiple jet array strategy over the single jet one. Figure 5 (b) shows that η^*_{jc} presents significantly larger values for the explored cooling capacity range. The combination of

two factors contribute to the pronounced increase of η^*_{jc}, i.e., lower values for the minimal second-law efficiency, η_{min}, and for the combined thermal resistance of the hot and cold ends ($R_{hs} + R_{amb}$) for the multiple jet array cases.

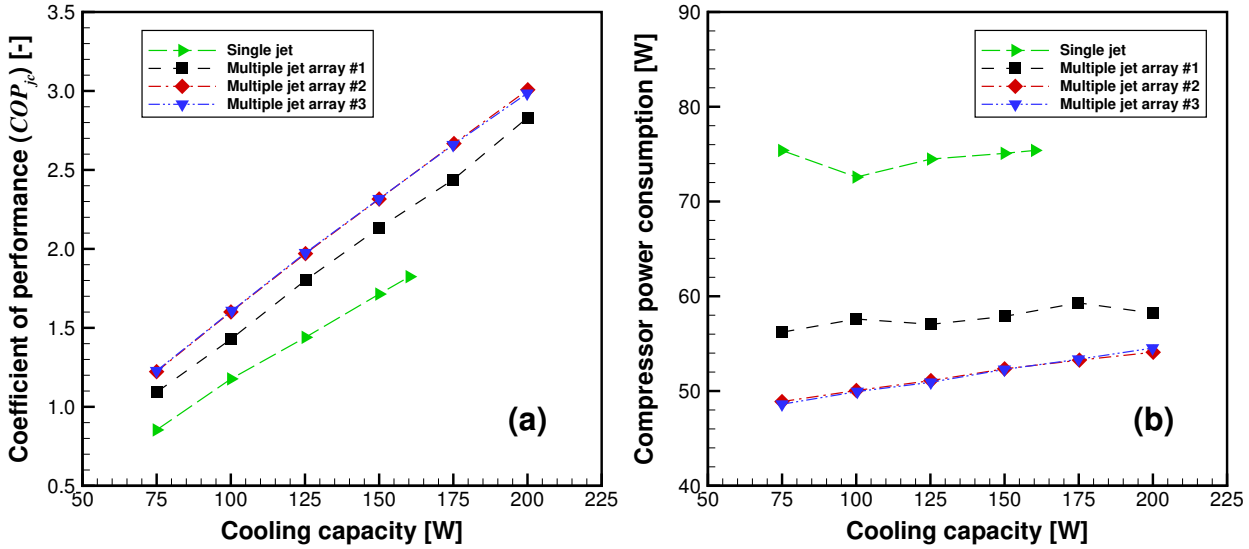

Figure 4: (a) Coefficient of performance and (b) compressor electrical power consumption as a function of the cooling load.

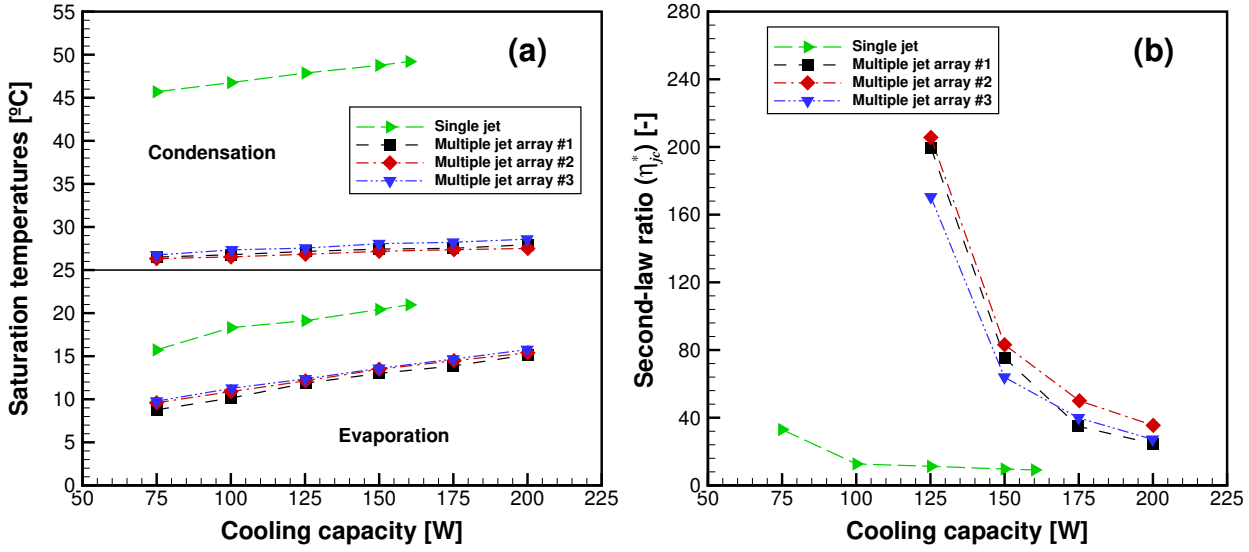

Figure 5: (a) Saturation temperatures and (b) second-law ratio as a function of the cooling load.

Since the multiple jet arrays #2 and #3 differ by a 45º rotation of the orifice configuration, it is expected that the heated surface temperatures will be similar, as revealed in Fig. 6 (a). This figure evinces that a more spaced jet array configuration is beneficial to reach lower surface temperatures, particularly at high cooling capacities. Compared to the single jet cooling scheme, the multiple jet arrays enabled the active cooling system to remove higher cooling loads while maintaining the surface temperature well below the conventionally established limit of 85ºC (Mudawar, 2001). For cooling loads up to 150 W, it is possible to see that the three multiple jet arrays present close values for the surface temperature. However, a sharp increase is clearly perceived for array #1 at higher cooling loads. This is an immediate consequence of the average jet impingement heat transfer coefficient decrease shown in Fig. 6 (b). After reaching the maximum point at 150 W, the average heat transfer coefficient of the multiple jet array #1 abruptly decreases whereas

for the remaining arrays the heat transfer coefficient also decreases, but at a more moderate rate.

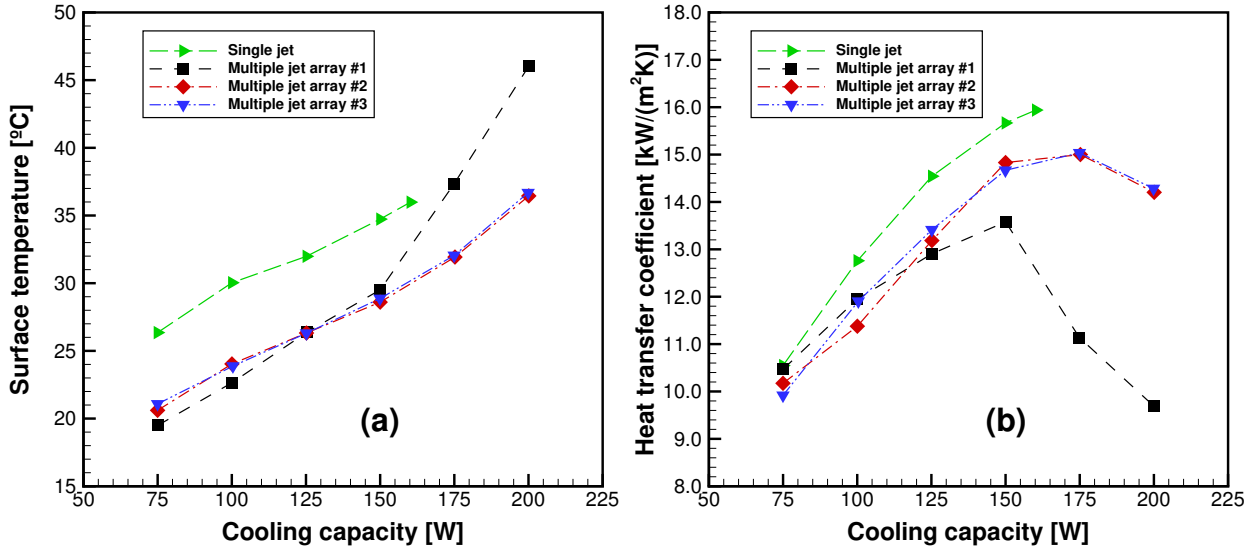

Figure 6: Jet cooler heat transfer parameters as a function of the cooling load, i.e., (a) surface temperature and (b) average jet impingement heat transfer coefficient.

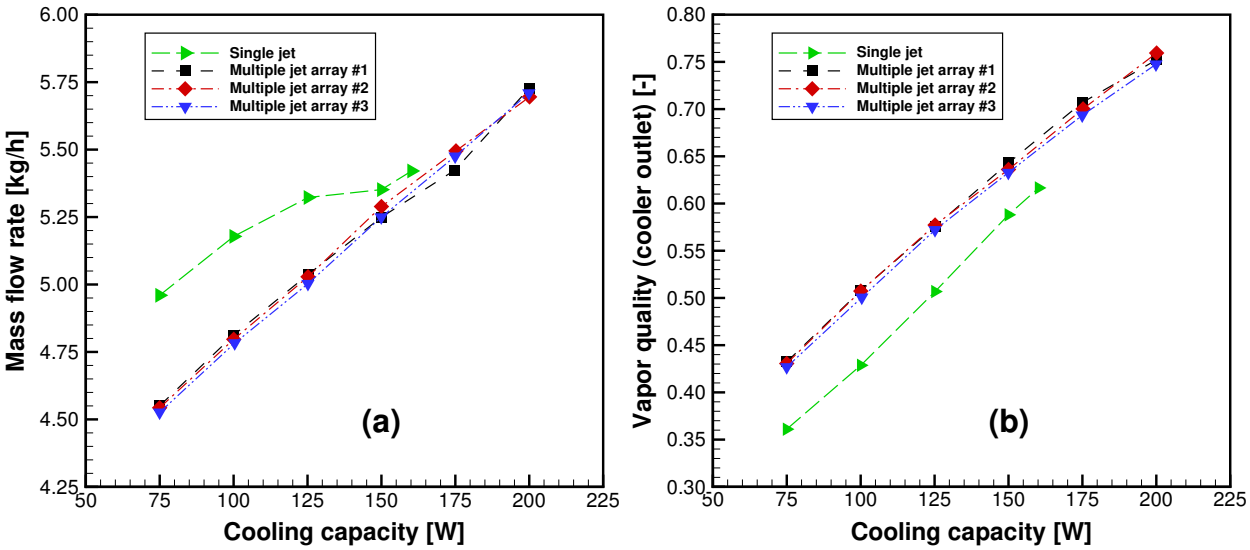

Figure 7: (a) Refrigerant mass flow rate and (b) vapor mass quality at the outlet of the jet cooler as a function of the cooling load.

Despite the higher surface temperature observed for the single jet-based tests, a combination of two factors may explain the higher values of the single jet-based average heat transfer coefficient compared to that of the multiple jet cases: (i) a higher mass flow rate as shown in Fig. 7 (a), and (ii) a lower outlet vapor mass quality, as evinced by Fig. 7 (b). The latter indicates a higher liquid mass flow rate flowing on the heated surface. It is important to mention that the refrigerant mass flow rate increases as a result of the increase in refrigerant density at the compressor inlet (due to the higher evaporating pressures that, in turn, increase with the cooling capacity). Interestingly, the different behavior of the average heat transfer coefficient for array #1 is not related to the vapor quality at the outlet of the jet cooler, as illustrated in Fig. 7 (b). The vapor quality increases steadily, exhibiting very close values for all multiple jet configurations as well as reaching very high values (up to 75%). An explanation for the average heat transfer coefficient

behavior for the multiple jet array #1 may lie in the fact that in this configuration the jets are positioned closer to each other and the impingement is concentrated at the center of the heated surface; a geometry that resembles the single-orifice impingement from the point of view of the heat transfer interaction. Besides, the outlet vapor quality can be interpreted as an evaporation efficiency (Xie *et al.*, 2014), as the liquid that leaves the jet cooler does not produce a cooling effect. Therefore, high evaporation efficiencies are observed (up to 75%), showing that the designed heat sink was capable of converting a large amount of the impinging liquid jet into vapor, which is the main physical mechanism responsible for the heat removal from the test surface.

5. CONCLUSIONS

A novel two-phase jet heat sink that integrates the evaporator and the expansion device into a single cooling module was presented. The new jet cooler was combined with a refrigeration system which operates with a compact oil-free linear motor R-134a compressor. The applicability of the system in the removal of highly concentrated heat loads was demonstrated. Experiments have been conducted for distinct jet configurations, i.e., single and multiple jet arrays. The influence of the applied thermal load, orifice number and geometric configuration on the system performance was quantified. In addition to the heater surface temperature and average two-phase jet impingement heat transfer coefficient, a comprehensive thermodynamic analysis was performed using different performance metrics.

For a fixed orifice diameter and a fixed jet length, operating the active cooling system with the multiple orifice configurations resulted in a better thermodynamic performance than the single orifice configuration. The combined effect of lower values for the minimal second-law efficiency and for the combined thermal resistance of the hot and cold reservoirs increased the second-law ratio considerably. The two-phase jet heat sink was capable of dissipating cooling capacities of up to 160 W and 200 W from a 6.36-cm^2 surface for single and multiple orifice configurations (#2 and #3), respectively. For these cases, the temperature of the impingement surface was kept below 40ºC and the heat transfer coefficient reached values between 14,000 and 16,000 W/(m^{2}K). The compact vapor compression cooling solution introduced here can be further developed for specific applications in thermal management of power electronics for a variety of stationary and mobile systems (for instance, hybrid and electric vehicles).

NOMENCLATURE

COP	coefficient of performance	(-)
h	specific enthalpy	(J/kg)
$\dot{m}_r$	refrigerant mass flow rate	(kg/h)
$\dot{Q}_c$	cooling capacity	(W)
$\dot{Q}_c^*$	corrected cooling capacity	(W)
R	thermal resistance	(K/W)
T	temperature	(ºC)
$\dot{W}$	input power, work rate	(W)
η	second-law efficiency	(-)
η^*	second-law ratio	(-)
φ	average heat transfer coefficient	(W/(m^{2}K))

Subscript

amb	ambient
comp	compressor
cond	condensing
evap	evaporating
hl	heat load
hs	heat sink
id	ideal (Carnot)
jc	jet cooler
s	surface
w,i	water-ethylene glycol at the condenser inlet

REFERENCES

Anandan, S. S., & Ramalingam, V. (2008). THERMAL MANAGEMENT OF ELECTRONICS: A REVIEW OF LITERATURE. *Thermal Science*, *12*(2), 5--26.

Barbosa Jr., J. R., & Hermes, C. J. L. (2006). HEAT TRANSFER IN REFRIGERATION APPLICATIONS. In G. F. Hewitt (Ed.), *Heat Exchanger Design Handbook - Heat Exchanger Design Updates* (1st ed., Vol. 13, p. 1-30). New York: Begel House, Inc.

Barbosa Jr., J. R., Ribeiro, G. B., & Oliveira, P. A. (2012). A State-of-the-Art Review of Compact Vapor Compression Refrigeration Systems and Their Applications. *Heat Transfer Engineering*, *33*(4--5), 356--374.

Bar-Cohen, A. (2013). Completing the Inward Migration - The Transformative Nature of Embedded Cooling. In *Proceedings of the HT2013.* Minneapolis, MN. (Keynote lecture)

Chu, R. C., Simons, R. E., Ellsworth, M. J., Schmidt, R. R., & Cozzolino, V. (2004). Review of Cooling Technologies for Computer Products. *IEEE Transactions on Device and Materials Reliability*, *4*(4), 568--585.

Chunqiang, S., Shuangquan, S., Changqing, T., & Hongbo, X. (2012). Development and experimental investigation of a novel spray cooling system integrated in refrigeration circuit. *Applied Thermal Engineering*, *33--34*, 246--252.

Hou, Y., Liu, J., Su, X., Qian, Y., Liu, L., & Liu, X. (2015). Experimental study on the characteristics of a closed loop R134-a spray cooling. *Experimental Thermal and Fluid Science*, *61*, 194--200.

Lemmon, E. W., Huber, M. L., & McLinden, M. (2007). *NIST Reference Fluid Thermodynamic and Transport Properties - REFPROP.* (Version 8.0)

Mancin, S., Zilio, C., Righetti, G., & Rossetto, L. (2013). Mini Vapor Cycle System for high density electronic cooling applications. *International Journal of Refrigeration*, *36*(4), 1191--1202.

Marcinichen, J. B., Olivier, J. A., Lamaison, N., & Thome, J. R. (2013). Advances in electronics cooling. *Heat Transfer Engineering*, *34*(5-6), 434--446.

Miner, A., & Ghoshal, U. (2006). Limits of Heat Removal in Microelectronic Systems. *IEEE Transactions on Components and Packaging Technologies*, *29*(4), 743--749.

Mudawar, I. (2001). Assessment of High-Heat-Flux Thermal Management Schemes. *IEEE Transactions on Components and Packaging Technologies*, *24*(2), 122--141.

Nakayama, W., Suzuki, O., & Hara, Y. (2009). Thermal Management of Electronic and Electrical Devices in Automobile Environment. In *Proceedings of the VPPC '09* (pp. 601--608). Dearborn, MI: IEEE.

Oliveira, P. A. (2016). *Development of a Two-Phase Jet Heat Sink Integrated with a Compact Refrigeration System for Electronics Cooling*. Dr. eng. thesis, Federal University of Santa Catarina. doi: 10.13140/RG.2.1.2602.2807/1

Ortega, A., & Birle, J. R. (2006). The evolution of air cooling in electronic systems and observations about its limits. In *Proceedings of the 18th National & 7th ISHMT-ASME HMTC.* Guwahati, India: ASME. (paper K10)

Whelan, B. P., Kempers, R., & Robinson, A. J. (2012). A liquid-based system for CPU cooling implementing a jet array impingement waterblock and a tube array remote heat exchanger. *Applied Thermal Engineering*, *39*, 86--94.

Xie, J. L., Tan, Y. B., Wong, T. N., Duan, F., Toh, K. C., Choo, K. F., … Chua, Y. S. (2014). Multi-nozzle array spray cooling for large area high power devices in a closed loop system. *International Journal of Heat and Mass Transfer*, *78*, 1177--1186.

Yan, Z. B., Toh, K. C., Duan, F., Wong, T. N., Choo, K. F., Chan, P. K., & Chua, Y. S. (2010). Experimental study of impingement spray cooling for high power devices. *Applied Thermal Engineering*, *30*(10), 1225--1230.

ACKNOWLEDGMENTS

This work was made possible through the financial investment from the EMBRAPII Program (POLO/UFSC EMBRAPII Unit - Emerging Technologies in Cooling and Thermophysics). Additional support from Embraco and CNPq (Grant No. 573581/2008-8 - National Institute of Science and Technology in Cooling and Thermophysics) is gratefully acknowledged.